J Bionic Eng 16 (2019) 337–353
DOI: https://doi.org/10.1007/s42235-019-0029-0

Journal of Bionic Engineering
http://www.springer.com/journal/42235

Effect of Different Reinforcing Fillers on Properties, Interfacial Compatibility and Weatherability of Wood-plastic Composites

Xiaoqian Wang[1,2], Zhiming Yu[1], Armando G. McDonald[2*]

1. *MOE Key Laboratory of Wooden Material Science and Application*, *Beijing Forestry University*, *Qinghua East Road No.*35, *Beijing* 100083, *China*

2. *Renewable Materials Program*, *Department of Forest*, *Rangeland*, *and Fire Sciences*, *University of Idaho*, 875 *Perimeter Drive MS* 1133, *Moscow*, *Idaho* 83844-1133, *USA*

Abstract

Utilization of biochar in plastic based blends offers a sustainable way to renewable materials as well as value-added use of wood waste. To investigate the interfacial compatibility and weatherability properties of biochar composites, four types of Wood-Plastic Composites (WPC) were prepared by an extrusion process. The mechanical properties, water absorptions, thermal and viscoelastic properties, and rheological behavior of the composites were also evaluated. The decolorizing carbon (NA) composite melts showed the higher modulus and viscosity, indicating better melt strength. The NA composites performed the best in tensile properties (strength of 28.6 MPa and modulus of 3.4 GPa) and had strong interfacial interaction between particles and the matrix. The degree of HDPE crystallinity in the biochar and carbon composites decreased relative to Douglas-fir (DF) composites, while the thermal properties of the composites improved compared with DF composites. For the water resistance, the DF composites displayed the highest water absorption (3.7%) and thickness swell (2.9%). During accelerated weathering tests, longer exposure time increased the color change and lightness, especially for DF composite. NA and biochar composites resulted in improved photostability. This study opens up a pathway to utilize effectively the renewable biochar as reinforcing filler in WPC in outdoor applications.

Keywords: biochar, interfacial compatibility, accelerated weathering, wood-plastic composites

1 Introduction

With the increasing worldwide demand for the limited forest resources in all kinds of applications, there is a severe shortage in wood supply[1]. Wood-Plastic Composites (WPC) are good alternatives to wood. WPC are commodity product used globally comprised of woody fibers from mill residues and recycled plastics[2]. Due to the low prices, easy availability, and adequate strength, WPC have been widely applied in decking products, furniture, fencing, playground equipment, and automotive components[3–5]. However, WPC have had major issues with material failing due to interfacial compatibility and weathering, and mainly contributed by the hydrophilic wood fiber[6]. The hydrophilic nature of wood fiber is attributed to the hydroxyl groups in cellulose, hemicellulose and lignin, which can induce water absorption, fiber swelling and weathering degradation[1,7].

In order to improve these properties mentioned above, researchers are concentrated on physical or chemical modification of wood, such as incorporation of nanoparticles[8,9], acetylation[7,10], and silane treatment[11]. However, there are disadvantages among these methods, such as environmental pollution, high cost, complicated processing techniques, and easy aggregation of nanoparticles in polymer matrix. On the other hand, because of the growing interest in renewability and cleaner production, bio-based natural reinforcements have increasingly attracted many researchers' attention recently[12]. Biochar is a carbon-rich co-product produced from pyrolysis of carbonaceous biomass at high temperature (400 ˚C – 700 ˚C) in an oxygen-depleted environment[13,14]. A slow pyrolysis process can produce slightly more biochar with a concomitant smaller amount of bio-oil[15]. On the other hand, fast pyrolysis has a high heating rate (> 300 ˚C·s^{-1}), resulting in higher yields of bio-oil and lesser amount of biochar[16]. Pyrolysis is a low cost option to reduce wood's (or lignocellulosic) hydrophilicity, therefore,

***Corresponding author:** Armando G. McDonald
E-mail: armandm@uidaho.edu

more water resistant and compatible with the hydrophobic matrix[17].

Biochar has many distinctive characteristics, *e.g.*, high adsorption capacity, high ion exchange, high surface area, high surface charge, high carbon sequestration, high nutrient exchange and large microporosity, thus, it is mainly used in the field of environmental remediation and soil amelioration[18–21]. Additionally, biochar is a value added waste, thermally stable and hydrophobic; therefore, pyrolysis biochar are potentially suitable hydrophobic reinforcing fibers. Zhang *et al*.[22] prepared biochar/wood/plastic composites with different biochar content and suggested that the appropriate amount of biochar can promote the mechanical properties. Das *et al*.[23] used pine wood biochar and polypropylene (PP) to make biocomposites and found that incorporation of biochar improved the mechanical and thermal properties. DeVallance *et al*.[24] combined biochar with PP and wood flour to prepare composite products, where they reported biochar could increase the mechanical properties and water resistance. Ho *et al*.[25] used bamboo charcoal as reinforcement for polylactic acid (PLA) and the mechanical, thermal and optical properties were enhanced. Ahmetli *et al*.[26] studied three different types of biochar as fillers with polyethylene terephthalate (PET) and concluded that the thermal and mechanical properties of neat epoxy resin were improved.

According to the previous studies, biochar, which is a good candidate as reinforcing fillers with polymer matrix, could improve the thermal, mechanical and optical properties for polymer matrix. However, very little attention has been paid to the composites' photostability and interfacial compatibility. In this study, we used biochar as reinforcing filler in HDPE to prepare the composites by an extrusion process. The DF and NA composites were also prepared as comparison. Thus, the aim of this study is to investigate the effects of biochar in comparison to wood particles and carbon on their photostability and interfacial property of wood-plastic composite. Moreover, the water absorption, thermal, rheological and mechanical properties were also investigated.

2 Materials and methods

2.1 Materials

High-density polyethylene (HDPE, Equistar petrothene, LB 0100-00) with a density of 0.950 $g \cdot cm^{-3}$ and a melt flow index of 0.3 g per 10 min and maleated polyethylene (MAPE) (Polybond 3029) were used as received. Douglas-Fir (DF) planar shavings were obtained from SDS Lumber Co., Bingen, WA and used as-is for the pyrolysis demonstration studies. Western Renewable Technologies (WRT) pyrolyzed DF using an auger reactor (6.8 $kg \cdot h^{-1}$, 5 min residence time) at 575 ˚C to obtain WRT biochar at 22% yield. Amaron Energy (AM) pyrolyzed DF in a rotary kiln reactor (12.2 $kg \cdot h^{-1}$, 10 min residence time) at 450 ˚C to obtain AM biochar at 25% yield. DF, WRT biochar and AM biochar were Wiley milled to pass through a 0.5 mm screen. Norit-A decolorizing carbon (NA) was purchased from Eastman Kodak Co., USA.

2.2 Composite preparation

DF, WRT biochar, AM biochar and NA were oven dried for 24 h at 104 ˚C prior to composites production. Fiber (50% w/w), HDPE (48% w/w) and MAPE (2% w/w) were blended in 500 g batches and then compounded/extruded using a 18 mm co-rotating twin-screw extruder (Leistritz, LD ratio 40, 200 rpm) into a ribbon (3.5 × 50 mm^2). The barrel and die temperatures were set between 140 ˚C and 160 ˚C. The ribbons were then hot pressed (300 × 300 mm^2, PHI press) slowly at 140 ˚C to 2 mm (weathering test) or 3 mm (mechanical and water soak tests) to obtain a flat material for specimen preparation.

2.3 Characterization

2.3.1 Particle characterization

Optical microscopy was performed on screened particles on an Olympus BX51 microscope equipment with a DP70 digital camera at 40 × magnification for DF and 100 × magnification for WRT/AM biochar and NA carbon. Particles measurements (length and width) were performed on 500 particles for each sample using the Olympus MicroSuite software[27]. The specific surface area (S_{BET}) of the samples were determined by N_2 physisorption (Micromeritics Flowmaster-II 3020). Before analysis, the samples were degassed at 104 ˚C for 24 h. The S_{BET} of the samples were calculated using the Brunauer-Emmett-Teller (BET) method.

The particles (~4 g) were Soxhlet extracted using

dichloromethane (CH_2Cl_2, 150 mL) for 24 h based on ASTM D1108. The extract was then concentrated using a rotary evaporator to constant weight and yield recorded gravimetrically.

2.3.2 Thermomechanical analysis (TMA) analysis

TMA of the biochar composite samples (2 × 1.5 × 1 mm^3) was carried out using a PerkinElmer TMA 7 instrument with a penetration probe at an applied static force of 10 mN from 30 ˚C to 200 ˚C at 5 ˚C·min^{-1}. The T_m was determined from the onset point of softening.

2.3.3 Dynamic Mechanical Analysis (DMA) analysis

DMA was performed on rectangular samples (60 × 9 × 3 mm^3) using a DMA Q800 (TA instruments) unit in the three-point bending mode from 30 ˚C to 120 ˚C at 2 ˚C·min^{-1}, 0.05% strain, and at 1 Hz frequency. Storage modulus (E') and damping factor (tanδ) data were recorded. The interfacial adhesion of the composites was evaluated by the adhesion factor (A):

$$A = \frac{1}{1-V_f}\frac{\tan\delta_c}{\tan\delta_m} - 1, \quad (1)$$

where c and m denote the composite and HDPE, respectively, and V_f is the fiber volume fraction which is calculated using:

$$V_f = \frac{W_f\rho_m}{W_f\rho_m + W_m\rho_f}, \quad (2)$$

where W_f is the weight of fiber (50%), W_m is the weight of HDPE (50%), ρ_m and ρ_f is the density of HDPE (0.950 g·cm^{-3}) and fiber (DF fiber: 1.5 g·cm^{-3}[28], WRT biochar: 1.5 g·cm^{-3}, AM biochar: 1.5 g·cm^{-3}, and NA carbon: 1.8 g·cm^{-3}[29], respectively.

2.3.4 Thermogravimetric analysis (TGA) analysis

The thermal stability of the DF fiber, biochar, NA carbon, and composites (5 mg) was determined by TGA using a PerkinElmer TGA 7 instrument. The samples were heated from 30 ˚C to 700 ˚C at a heating rate of 20 ˚C ·min^{-1} under nitrogen (30 mL·min^{-1}).

2.3.5 Differential Scanning Calorimetry (DSC) analysis

DSC was performed on samples (3 mg – 4 mg) using a TA Instrument model Q200 DSC under nitrogen (20 mL·min^{-1}). The samples were first equilibrated at 20 ˚C (3 min), and then ramped to 180 ˚C at 10 ˚C·min^{-1} (cycle 1); cooled to 20 ˚C at −10 ˚C·min^{-1} (cycle 2); then reheated to 180 ˚C at a rate of 10 ˚C·min^{-1} (cycle 3). The degree of crystallization (X_c) was calculated by:

$$X_c = \frac{\Delta H_m}{\Delta H_0 \times W_f} \times 100\%, \quad (3)$$

where ΔH_m represents the melting enthalpy which was calculated from the area under the peak observed at cycle 3, ΔH_0 is the theoretical fusion enthalpy of a 100% crystalline HDPE (293 J·g^{-1}), and W_f is the weight fraction on HDPE in the composites (50%).

2.3.6 Dynamic rheological analysis

Parallel plate (25 mm Ø, serrated) dynamic rheological measurements (elastic modulus (G'), viscous modulus (G'') and complex viscosity (η^*)) on composite samples (2.5 mm × 25 mm Ø) were evaluated with the Bohlin CVO 100 N rheometer equipped an extended temperature unit using an angular frequency from 0.01 Hz to 100 Hz with 0.5% strain and at 180 ˚C. Melt Flow Rate (MFR) of the composite samples (4.0 g, 4 replicates) was conducted through a die (8 mm × 2.0955 mm Ø) at a temperature of 190 ˚C and load of 15 kg. The MFR of the samples were measured according to ASTM D 1238-01e1 (2008) using CEAST Modular Melt Flow Indexer (Model 7024.000).

2.3.7 Contact Angle (CA) and water absorption analysis

CA measurements on composite samples (100 × 15 × 2 mm^3) were carried out with a Thwing-Albert PG-2 Pocket Goniometer using the sessile water drop method. Data were processed with the Pocket Goniometer v3.3 software. Water Absorption (WA) and Thickness Swell (TS) measurements on composite samples (50 × 30 × 3.0 mm^3, 4 replicates) were conducted at 23 ˚C for 70 d. The weight and dimensions of the samples were measured before and after soaking. The diffusion coefficients (D_f) of the composite samples were calculated using:

$$D_f = \pi(h/4M_\infty)^2(\Delta M/\Delta t^{1/2})^2, \quad (4)$$

where M_∞ is the maximum Moisture Content (MC) measured at the end of the test, h is the sample thickness

corresponding to M_∞, t is the time, and $\Delta M/\Delta t^{1/2}$ is the initial slope from the MC versus $t^{1/2}$ relation.

2.3.8 Tensile property analysis

Tensile tests were performed on machined dog-bone specimens (8 replicates) according to ASTM D 638, using an Instron 5500R-1132 universal test machine with load cell of 5 kN and crosshead speed of 5 mm·min^{-1}. The strain was measured with an extensometer (model 3542, Epsilon Technology Corp).

2.3.9 Accelerated weathering analysis

Accelerated weathering was conducted in a xenon-arc weatherometer (Q-Sun Xe-1-S). Composite specimens (2 × 40 × 60 mm^3) were lightly sanded and then subjected to an accelerated weathering procedure in accordance with ASTM D 6662 standard and Fabiyi and McDonald[30]. The average irradiance was 0.70 W·m^{-2} at 340 nm with a chamber temperature of 70 ˚C and water spray. The color change and chemical characterization of the samples were collected between 0 h and 1200 h. Color parameters of weathered samples (4 replicates) were recorded using a Precise Color Reader (WR-10QC) with illuminant D65 and a 10˚ standard observer. The total color difference (ΔE^*) was calculated as:

$$\Delta L^* = L_1^* - L_0^*, \tag{5}$$

$$\Delta a^* = a_1^* - a_0^*, \tag{6}$$

$$\Delta b^* = b_1^* - b_0^*, \tag{7}$$

$$\Delta E^* = (\Delta L^{*2} + \Delta a^{*2} + \Delta b^{*2})^{1/2} \tag{8}$$

where ΔE^* represents the total color difference, L^* stands for the lightness and darkness of color, a^* indicates the redness and greenness of color, b^* denotes the yellowness and blueness of color, ΔL^*, Δa^*, and Δb^* are the differences of the composite sample values before and after treatment of L^*, a^*, and b^*, respectively.

2.3.10 Fourier transform infrared spectroscopy (FTIR) analysis

Surface chemistry of the weathered composites (4 replicates) was determined by FTIR spectroscopy using a Nicolet-iS5 spectrometer (ThermoScientific) equipped with a Ge crystal Attenuated Total Reflection (ATR) accessory (iD5). The spectra were baseline corrected and averaged using the Omnic v9.0 software (ThermoScientific). The concentrations of carbonyl (C=O) and vinyl (C=C) groups of the weathered samples can be calculated based on:

$$A^* = \varepsilon bc, \tag{9}$$

where A^* is the absorbance of the functional groups band, c is the molar concentration of the functional group mol·L^{-1} (M), ε is the molar absorptivity (L·mol^{-1}·cm^{-1}), and b is the path length of the sample (the optical path of the infrared beam through the sample, cm). To account for the carbonyl groups (1800 cm^{-1} – 1680 cm^{-1}) presented in the weathered composite samples, carbonyl index (*CI*) was calculated. *CI* was taken as the ratio of the area of carbonyl groups to the band area of –CH_2– groups (2917 cm^{-1} – 2912 cm^{-1}). The latter band was selected as a reference due to the stability during weathering[31].

3 Results and discussion

3.1 Fiber properties

The particle dimensions for the DF, WRT and AM biochar and NA carbon were determined by optical microscopy (Fig. 1 and Table 1). The length and width for DF were respectively 177 μm ± 27 μm and 38.5 μm ± 2.8 μm (Fig. 1a). The WRT biochar, AM biochars, and NA carbon were uniform in shape. The particle sizes of WRT biochar (Fig. 1b), AM biochars (Fig. 1c), and NA carbon (Fig. 1d) were respectively, 29.4 μm ± 6.5 μm, 25.4 μm ± 2.6 μm, and 11.1 μm ± 0.9 μm.

The surface area of DF was low at 0.9 m^2·g^{-1} and upon pyrolysis marginally increased (1 m^2·g^{-1} – 2 m^2·g^{-1}) and were unexpectedly low, suggesting a mild pyrolysis reaction occurred for both samples[29]. In contrast, the NA carbon had a large surface area of 750 m^2·g^{-1} and consistent with the Ref. [32].

Wood extractives can play a major role as a plasticizing agent in WPC to reduce melt viscosity and therefore necessary to know their levels[33]. The fiber sample had CH_2Cl_2 extractives contents ranged from 0.5% to 2.2% (Table 1). The DF CH_2Cl_2 extractives levels was lower than reported for Douglas-fir heartwood at 5.25%[30]. At these levels, the extractives are not expected to play a major role in melt properties[33].

Table 1 Particle size, surface area (S_{BET}), and extractives contents for the various fiber samples

Fiber sample	Particle size		S_{BET} ($m^2 \cdot g^{-1}$)	Extractive content (%)
	Length (μm)	Width (μm)		
DF fiber	177 (27)	38.5 (2.8)	0.9	1.59
WRT biochar	29.4 (6.5)		2.1	1.70
AM biochar	25.4 (2.6)		1.0	2.18
NA carbon	11.1 (0.9)		749	0.52

3.2 Composite melt properties

The Melt Flow Rates (MFR) and apparent viscosity of DF, AM biochar and WRT biochar composite samples (Table 2) were between 0.83 g to 2.70 g per 10 min and 27.2 kPa·s to 88.9 kPa·s, respectively. These values compared favorably for the WPC with those reported by Gallagher and McDonald[34] (0.35 g – 2.90 g per 10 min; 12.7 kPa·s – 107.0 kPa·s), Wei *et al.*[7] (1.55 g – 2.19 g per 10 min; 25.1 kPa·s – 35.2 kPa·s) and Adefisan and McDonald[27] (1.31 g – 1.60 g per 10 min; 46.5 kPa·s – 57.1 kPa·s). Statistical analysis showed that MFR of the three type's fiber was significantly different. The DF composite has the highest MFR and lowest melt viscosity. MFR measurements for the NA composite sample were not able to be obtained due to its very low displacement, even with a load of 15 kg.

The dynamic rheological behavior (elastic modulus (G') and viscous modulus (G'')) of HDPE and composite melts are shown in Fig. 2a. At low frequency, the G'' was higher than G' for HDPE, showing a liquid viscoelastic behavior[35]. For the WPC, G' was larger than G'' at low frequency regions, indicating an elastic response in the molten state, due to the fact that the polymer chains had sufficient time to show an elastic deformation rather than relaxation at low frequencies[36]. A similar phenomenon was also observed in wood flour (50%)/PP composites or wood flour (70%)/HDPE compared with other concentrations of wood flour composites due to the increased interactions between filler and matrix at high filler loadings and low frequencies[37,38].

The complex viscosity (η^*) was shown to decrease as the frequency increased, showing a shear thinning behavior of the HDPE matrix in the composites (Fig. 2b). The composite samples have higher η^* than HDPE, which is due to the formation of network-like structure in the composite melts[39]. Consequently, the composites showed a solid-like behavior because of the restrained motion of HDPE chains. The higher viscosity of NA composite could be explained by a higher fiber-matrix interaction in the melt due to a higher surface area for NA. A similar phenomenon has been observed in Ethylene Vinyl Acetate (EVA) copolymer filled with bamboo charcoal. The η^* of EVA increased after loading

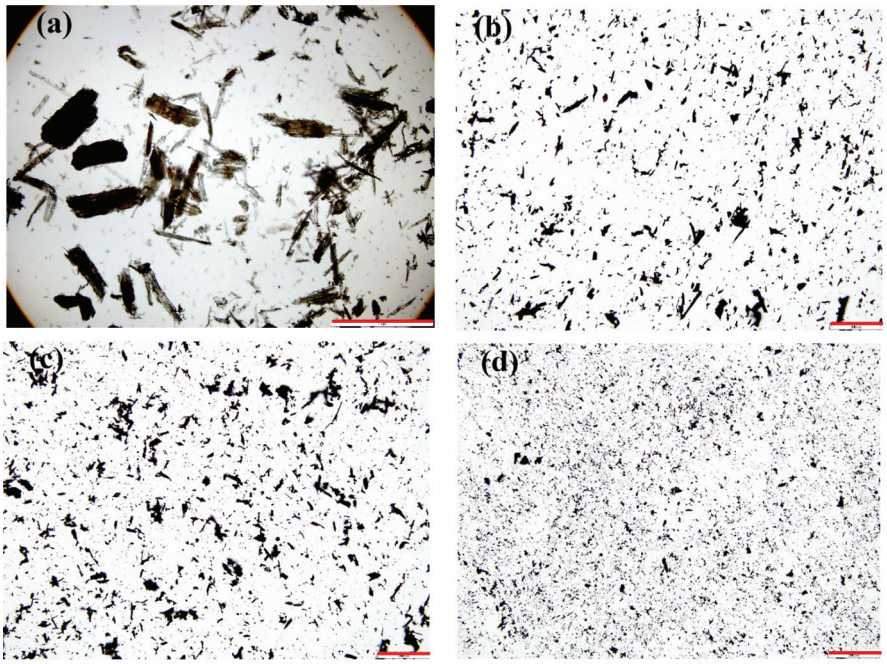

Fig. 1 Optical micrographs of (a) DF fiber (40×, scale bar 1 mm); (b) WRT biochar (100×, scale bar 200 μm); (c) AM biochar (100×, scale bar 200 μm), and (d) NA carbon (100×, scale bar 200 μm).

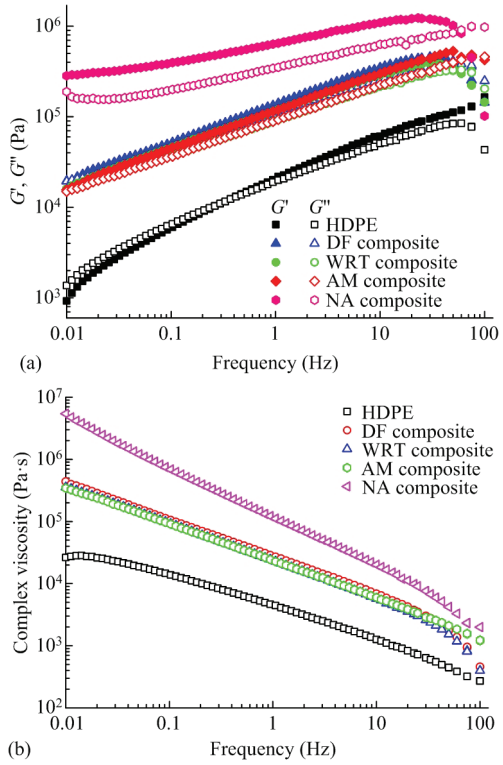

Fig. 2 (a) Dynamic rheology elastic (G') and viscous modulus (G''), and (b) complex viscosity (η^*) of HDPE and composite samples with frequency at 180 ˚C.

Table 2 Melt Flow Rates (MFR) and apparent viscosity at 190 ˚C and dynamic complex viscosity (η^*) at 180 ˚C of the composite samples

Samples	MFR (g per 10 min)	Apparent viscosity (kPa·s)	η^* at 1 Hz (MPa·s)
HDPE	–	–	4.4 (0.0)^c
DF composite	2.70 (0.19)^a	27.2 (2.0)^c	26.0 (1.5)^b
WRT composite	0.83 (0.05)^c	88.9 (5.0)^a	21.9 (1.3)^b
AM composite	1.23 (0.08)^b	59.7 (3.6)^b	18.2 (6.4)^b
NA composite	–	–	105.3 (8.1)^a

Note: Values in parentheses are standard deviations. Samples with different letters (a, b and c) are statistically significantly different ($p < 0.05$) using one-way ANOVA test.

the bamboo charcoal, and with the increasing bamboo charcoal loading, the η^* increased[40].

At low frequencies (< 1 Hz), the difference of η^* among DF composites, WRT composites, and AM composites was negligible, but η^* values of DF composites was slightly higher than the biochar composites. The η^* (at 1 Hz) was also shown to increase from 4.4 MPa·s for HDPE to 26.0 MPa·s for DF composite, 21.9 MPa·s for WRT composite, 18.2 MPa·s for the AM composite, and 105.3 MPa·s for the NA composite. The higher G' and η^* of NA composite suggested the better interfacial interaction between carbon particle and matrix and better melt strength[36].

3.3 Mechanical properties

Tensile modulus was significantly higher for all the composite samples compared to HDPE. The NA composites showed the highest tensile modulus (3.4 GPa), indicating a good interfacial adhesion and leading to better stress transfer efficiency from the HDPE matrix to the carbon filler. This is likely attributable to NA high surface area results in good interaction with the matrix. The tensile strength of AM composite and WRT composite decreased respectively by, 3% and 24% lower than HDPE (21 MPa). A similar result was found in the bamboo charcoal composite[1]. Furthermore, the DF composite has a higher tensile strength compared to the AM and WRT biochar composites. One reason could be that DF had a higher aspect ratio (~4.6) than the biochar (~1) which would improve reinforcement of the composite[41]. Ikram *et al.*[42] suggests that the biochar cannot chemically react with HDPE due to lack of surface functional groups especially hydroxyl groups. Das *et al.*[43] also reported similar results. However, Zhang *et al.*[44] found the tensile strength of rice husk biochar/HDPE composites were higher than rice husk power/HDPE composites, where they reported no hydrophilic hydroxyl functional group in the interior was beneficial to the interfacial bonding between biochar and HDPE. Moreover, the NA composite exhibited the highest tensile strength (28.6 MPa) and was the most hydrophobic as described in section **3.5**.

The composite samples' toughness was assessed by its Energy At Break (EAB) (Table 3). EAB of all the composite samples decreased compared to HDPE. The EAB values of composite samples were significantly lower (0.3 J – 0.9 J) than that of HDPE (4.2 J). Moreover, the EAB of NA composite decreased by 78% as compared to HDPE.

3.4 Thermal analysis

The viscoelastic properties (E' and tan δ) of HDPE and composite samples were evaluated using DMA in three-point bending mode. As can be seen from Fig. 3a, the E' of the composite samples decreased with temperature. This phenomenon was assigned to the low

Table 3 Density and tensile properties of composites made with DF fiber, AM biochar, WRT biochar and NA carbon

Samples	Density ($g \cdot cm^{-3}$)	Tensile strength (MPa)	Tensile modulus (GPa)	EAB (J)
HDPE	0.950	21.1 (0.4)^{b}	0.6 (0.0)^{c}	4.24 (0.46)^{a}
DF composite	1.026 (0.018)^{b}	21.5 (4.1)^{b}	2.3 (0.5)^{b}	0.75 (0.34)^{b}
WRT composite	1.027 (0.024)^{b}	16.1 (3.7)^{c}	2.0 (0.5)^{b}	0.32 (0.04)^{c}
AM composite	1.018 (0.053)^{b}	20.5 (3.5)^{b}	2.2 (0.3)^{b}	0.33 (0.12)^{c}
NA composite	1.090 (0.037)^{a}	28.6 (0.9)^{a}	3.4 (0.3)^{a}	0.93 (0.26)^{b}

Note: Values in parentheses are standard deviations. Samples with different letters (a, b and c) are statistically significantly different ($p < 0.05$) using one-way ANOVA test.

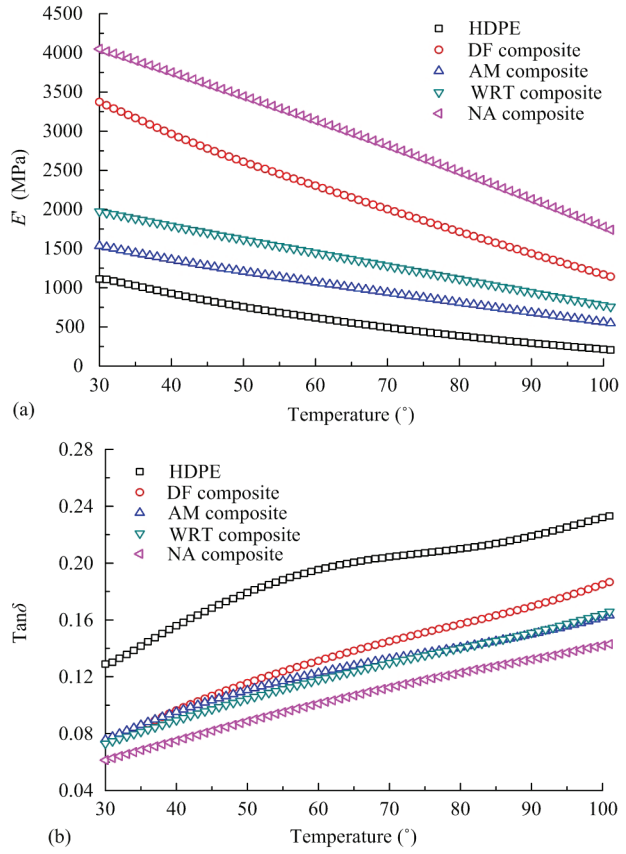

Fig. 3 (a) Storage modulus (E'), and (b) damping factor (tanδ) of HDPE and composite samples.

kinetic energy and high rigidity of the composites at low temperatures, and HDPE matrix softening causing relaxation in the composites at high temperatures[45,46]. Among the composite samples, the NA composite exhibited the maximum E' values, which may be attributed to the fact that the higher surface area of carbon led to stronger interactions with the matrix, and thus the motion of polymer system was restrained. At 30 ˚C, the E' of NA composite was 4.05 GPa, while for DF, AM and WRT composites were 3.4 GPa, 1.5 GPa and 2.0 GPa, respectively.

Tanδ is a measure of the energy dissipation of materials under cyclic load, and can be used to determine the internal bonding of composites. In Fig. 3b, within the measured temperature range, tanδ increased with temperature, resulting from a decrease in E' and increase in loss modulus (E'')[36]. The NA composite showed the lowest tanδ values, indicating the enhanced interactions and modified stress transfer[47]. The adhesion factor (A) was calculated to evaluate quantitatively the interaction between the reinforcing agent and the matrix. The lower values of A for the composite samples, the stronger interaction between the filler and matrix[48]. The A values for the samples at 30 ˚C, 50 ˚C, and 70 ˚C are given in Table 4. The NA composite had the lowest A values (or strongest interfacial interaction between particles and HDPE), followed by WRT composite. This could be ascribed to an increased surface hydrophobicity of these two wood fiber and are consistent with a high contact angle described later[7]. The A values at 30 ˚C were −0.278 for NA composite, −0.076 for WRT composite, −0.063 for DF composite, and −0.038 for AM composite, respectively.

The softening temperature (T_s) or melting temperature (T_m) of HDPE and composite samples was measured by TMA because of its sensitivity and ease of use[49]. The changes of the samples height (%) with the temperature (30 ˚C – 200 ˚C) are shown in Fig. 4, and the T_s was obtained from the onset point of samples softening. The T_s was measured to evaluate the chain entanglements between polymer matrix and reinforcing materials[50–52]. In general, the T_s tends to increase with the chain entanglements forming[53]. The T_s of HDPE, DF composite, WRT composite, AM composite, and NA composite was determined to be about 129 ˚C, 133 ˚C, 132 ˚C, 131 ˚C, and 134 ˚C, respectively. The T_s of composite samples was slightly higher than that of HDPE, maybe resulted from the interactions between wood fiber and matrix influencing the crystalline structure of HDPE. The incorporation of fiber made the sample more elastic in comparison with neat HDPE, which may contribute to the increase of T_s.

Table 4 tanδ and adhesion factor (A) values for HDPE, DF composite, WRT composite, AM composite, and NA composite at 30 ˚C, 50 ˚C, and 70 ˚C

Sample	$\tan\delta_{30\,^\circ C}$	$A_{30\,^\circ C}$	$\tan\delta_{50\,^\circ C}$	$A_{50\,^\circ C}$	$\tan\delta_{70\,^\circ C}$	$A_{70\,^\circ C}$
HDPE	0.129	–	0.179	–	0.204	–
DF composite	0.074	−0.063	0.116	0.059	0.145	0.161
WRT composite	0.073	−0.076	0.105	−0.042	0.130	0.041
AM composite	0.076	−0.038	0.111	0.013	0.133	0.065
NA composite	0.061	−0.278	0.089	−0.240	0.113	−0.095

DSC was performed to obtain information on the melting and crystallization behavior of HDPE in the composite. DSC thermograms of the cooling and second heating scans of HDPE and composite samples are shown in Fig. 5, and the corresponding parameters of thermal transitions including melting and crystallization are presented in Table 5. In the second heating scan, a typical melting peak at 131.0 ˚C was observed in HDPE. The T_m of composite samples was around 129 ˚C – 132 ˚C, and in the range of T_m determined by TMA. Moreover, NA composite had the lowest T_m of 129.5 ˚C. The crystallization temperature (T_c) is an important parameter to describe the crystallization behavior of HDPE and composite samples. The higher the T_c, the faster the crystallization of polymers[54]. For composite samples, the T_c of DF composite, WRT composite, AM composite, and NA composite were 118.9 ˚C, 118.3 ˚C, 117.7 ˚C, and 118.9 ˚C, respectively, slightly lower than that of HDPE (119.0 ˚C), suggesting wood fiber marginally hindered the crystallization process of HDPE (Table 5). A possible explanation is that wood fibers limit the flow of polymer, and restrict its rearrangement. The results are in agreement with Cui *et al.*[55] and contradicts the finding of Das *et al.*[56] and Ndiaye *et al.*[57]. Cui *et al.*[55] found addition of wood fiber in polymer composites delayed exothermic crystallization, whereas Das *et al.*[56] and Ndiaye *et al.*[57] observed the shifting of crystallization point to a higher temperature. The enthalpy of HDPE during crystallization (ΔH_c) was reduced by adding wood fiber. The crystallinity of WRT composite (59%), AM composite (55%) and NA composite (41%) was lower than that of DF composite (65%).

The thermal degradation behavior of the DF fiber, biochar, NA carbon, and composites was determined by TGA (Fig. 6a) and DTG (Fig. 6b). The char residue of DF fiber, WRT biochar, AM biochar, and NA carbon were 0.3%, 7.9%, 2.5%, and 13.5%, respectively (Fig. 6c). The weight loss of AM composite, WRT composite, and NA composite due to thermal degradation was observed in four distinctive stages (α, β, χ, and ω), however, an additional fifth stage (ψ) was occurred in the DF composite between 240 ˚C and 700 ˚C (Fig. 6a and Table 6). In the case of DF composite, the first (α), second (β), and third (χ) stages were corresponded to the degradation of hemicellulose, cellulose, and lignin, respectively[1,58–60]. The fourth (ω) and fifth (ψ) stages were attributed to the degradation of C–C bonds of HDPE[30]. The NA composite began to degrade at 290 ˚C, while the other composite samples started at 281 ˚C (DF

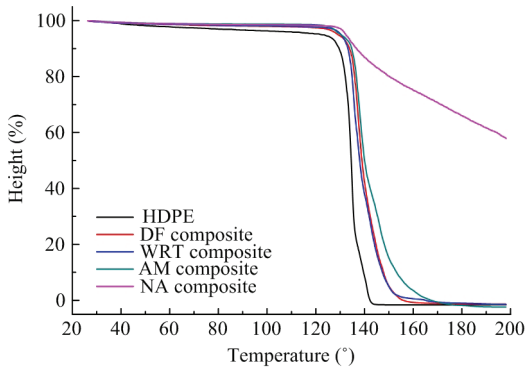

Fig. 4 TMA thermograms of HDPE, DF composite, WRT composite, AM composite, and NA composite.

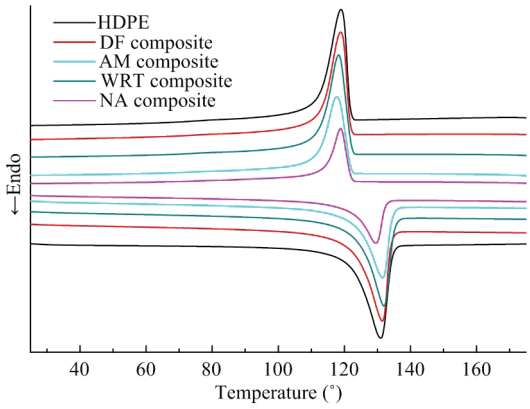

Fig. 5 DSC thermograms of the cooling and 2nd heating cycles of HDPE and composite samples.

Table 5 Calorimetric data for HDPE and composite samples

Samples	DSC				TMA
	T_c (°C)	T_m (°C)	X_c (%)	ΔH_c (J·g^{-1})	T_s or T_m (°C)
HDPE	119.0	131.0	61	172	129
DF composite	118.9	131.5	65	90	133
WRT composite	118.3	132.0	59	86	132
AM composite	117.7	131.5	55	71	131
NA composite	118.9	129.5	41	52	134

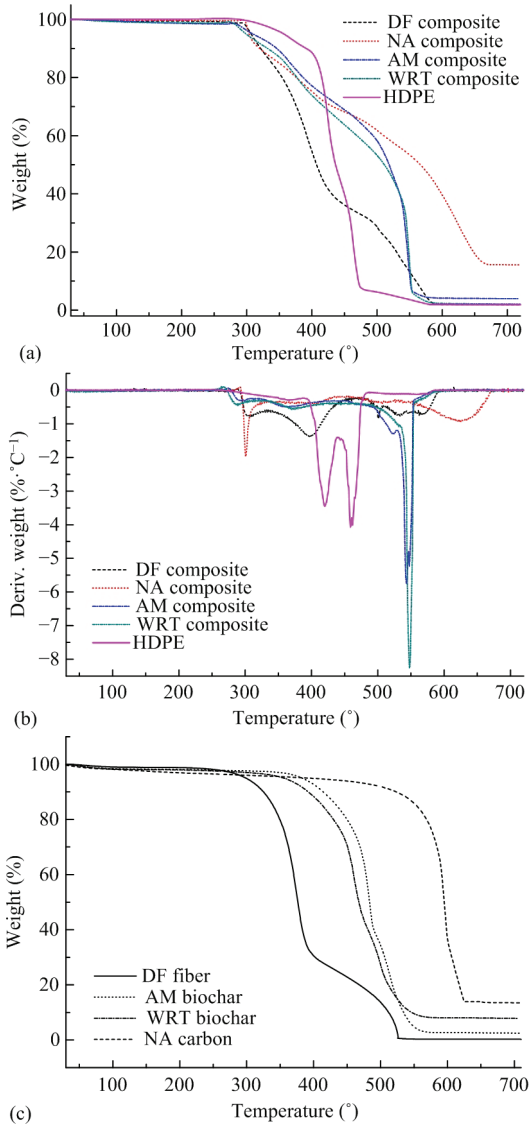

Fig. 6 (a) TGA and (b) DTG thermograms of HDPE, DF composite, WRT composite, AM composite, and NA composite; (c) TGA of DF fiber, WRT and AM biochar, and NA carbon.

composite), 275 °C (AM composite), and 266 °C (WRT composite), respectively. In addition, the char residue of NA composite was 15.6% at 700 °C, higher than that of the other composite samples. Thus, the NA composite had the better thermal stability than the other three composites. Moreover, the char residue of AM composite (4.0%) and WRT composite (2.1%) were higher than DF composite (1.9%) due to the decrease of the degradable components in biochar (cellulose, hemicellulose, and lignin)[61]. Compared with HDPE, the initial temperature and char residue of the NA composite, AM composite, and WRT composite increased, indicating that the addition of biochar and carbon to HDPE could improve the thermal stability of the composites. This finding was consistent with the literatures[62–64].

3.5 Physical properties

Water contact angle is a measure of the hydrophobicity of a surface. The average water contact angles at 30 s decreased in the following order: NA composite (106°) > WRT composite (105°) > AM composite (93°) > DF composite (87°) > HDPE (81°). This result shows that NA composite and WRT composite was notably more hydrophobic than the other three. This may contribute to more pronounced adhesion or compatibility for the NA carbon and WRT biochar with HDPE. The increased surface hydrophobicity of these two fiber types could contribute to the lowest A values (more compatible) of NA composite, followed by WRT composite, which was discussed earlier. The contact angles of NA composite, WRT composite and AM composite samples increase ≤ 1 s, and then stabilize after the water droplet drops onto the surface. On the other hand, the increase of fibers' char residue, which was discussed in the thermal analysis section **3.4**, could also contribute to the increase of the surface hydrophobicity.

Water soak tests assess the water ingress into the composite material and how this material would behave in a wet environment. During 70 d of immersion, the Water Absorption (WA) and thickness well (TS) were measured with time (Fig. 7 and Table 7). The WA at 70 d for DF, WRT, AM and NA composites were respectively, 3.7%, 2.0%, 1.7% and 1.3%. The biochar and carbon composites had better water resistance than the DF composite. The TS for these composites showed a similar trend to the WA results. This can be explained as follows: firstly, biochar contains numerous pores and gaps in its structure, and the pores and gaps were filled by HDPE; second, biochar is dispersed homogeneously in the matrix[1]. The results were also consistent with the contact angle test, which showed that the contact angle

Table 6 Thermal decomposition temperatures and residue content of composite samples

Samples	Temperature (°C)															Residue at 700 °C (%)
	First stage			Second stage			Third stage			Fourth stage			Fifth stage			
	α_1	α_2	T_{max}	β_1	β_2	T_{max}	χ_1	χ_2	T_{max}	ω_1	ω_2	T_{max}	ψ_1	ψ_2	T_{max}	
HDPE	260	364	383	364	440	420	440	588	459	–	–	–	–	–	–	1.88
DF composite	281	335	305	335	468	396	468	511	501	511	554	533	554	607	568	1.89
NA composite	290	341	301	341	450	404	450	534	501	534	690	626	–	–	–	15.62
AM composite	275	315	295	315	445	364	445	529	523	529	584	543	–	–	–	3.95
WRT composite	266	308	285	308	437	362	437	513	509	513	616	532	–	–	–	2.12

Note: [1] and [2] refer to the temperatures of the first onset and final decomposition.

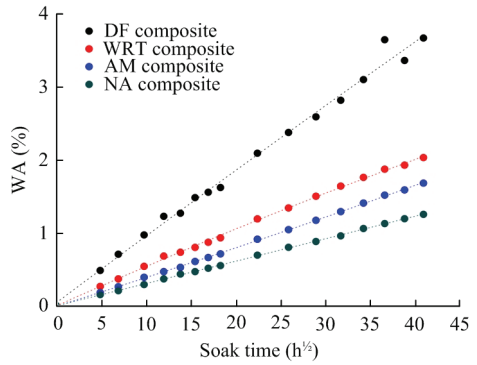

Fig. 7 Water absorption of composite samples as a function of soak time$^{1/2}$.

between water and biochar/carbon was higher than between the DF fiber surface. Water absorption rates of the composite samples were measured with Fick's law of diffusion model by plotting water absorbed versus time$^{1/2}$ using a polynomial curve fitting at 2nd order[65]. The D_f for DF, WRT, AM, and NA based composites were 4.60 $m^2 \cdot s^{-1}$, 3.98 $m^2 \cdot s^{-1}$, 2.34 $m^2 \cdot s^{-1}$, and 4.06 × 10^{-13} $m^2 \cdot s^{-1}$, respectively. The higher D_f, the shorter time taken to reach the equilibrium MC[49].

3.6 Accelerated weathering studies

Accelerated weathering was performed to assess the in-service performance of these biochar/carbon filled composite materials. Initially, the samples were visually inspected by reflectance microscopy. The accelerated weathered DF composite samples whitened after 1200 h of exposure time (Fig. 8a). After 400 h of exposure, the content of wood fiber on the DF composite surface decreased, making the surface white. After 800 h of weathering, only a small amount of fiber was left on the wood composite surface. When the exposure time was further increased (1200 h), the number of wood fibers at the surface continually decreased and the color was almost white. Wei *et al.*[7] also found a similar phenomenon. However, the visual color of WRT composite (Fig. 8b), AM composite (Fig. 8c), and NA composite (Fig. 8d) changed slightly. This result indicated that the biochar and carbon composites were more apparently photostable than the DF composite. The micrographs of the biochar/carbon composites show a white crystalline appearance because the samples were lightly sanded before testing; however, the samples were very dark in color. Therefore, color measurements were taken to monitor changes in the samples.

The color changes (ΔE^*), color lightness (ΔL^*), redness and greenness (Δa^*), and yellowness and blueness (Δb^*) of weathered HDPE and WPC are shown in Fig. 9. ΔL^* can be used to measure the degree of weathered composite relative to the original composite surface color. The color changes (Fig. 9b) and surface color lightness (Fig. 9a) of DF composite increased rapidly and significantly, while the WRT and AM composites increased slowly and slightly. The NA composite had the lowest ΔE^* and ΔL^* changes, indicating that the NA composite had better apparent resistance to photodegradation (Figs. 9a and 9b). For instance, when the exposure time elapsed 1200 h, the ΔE^* and ΔL^* of DF composite were 37.87 and 36.68, while the ΔE^* and ΔL^* of NA composite were 0.83 and −0.71, respectively. The ΔE^* and ΔL^* ranked as the following order: NA composite < WRT composite < AM composite < DF composite. Javadi *et al.*[66] studied the effect of CB and Hindered Amine Light Stabilizer (HALS) hybrid systems on the UV stability of HDPE. They concluded that both CB (blocked light) and HALS improved the stability through completely different mechanisms. Liu and Horrocks[67] found that the size of CB particles influenced their performance greatly, and the smaller

Table 7 Water absorption (*WA*), thickness swell (*TS*), and Fick's diffusion coefficient (D_f) of composite samples

Samples	*WA* (%)		*TS* (%)		D_f (10^{-13} $m^2 \cdot s^{-1}$)
	1 d	70 d	1 d	70 d	
DF composite	0.48 (0.04)	3.67 (0.35)	0.99 (0.82)	2.88 (0.86)	4.60
WRT composite	0.26 (0.04)	2.03 (0.17)	0.75 (0.75)	2.79 (1.06)	3.98
AM composite	0.18 (0.01)	1.68 (0.03)	0.92 (1.00)	2.74 (1.25)	2.34
NA composite	0.15 (0.02)	1.25 (0.02)	0.36 (0.36)	1.87 (0.39)	4.06

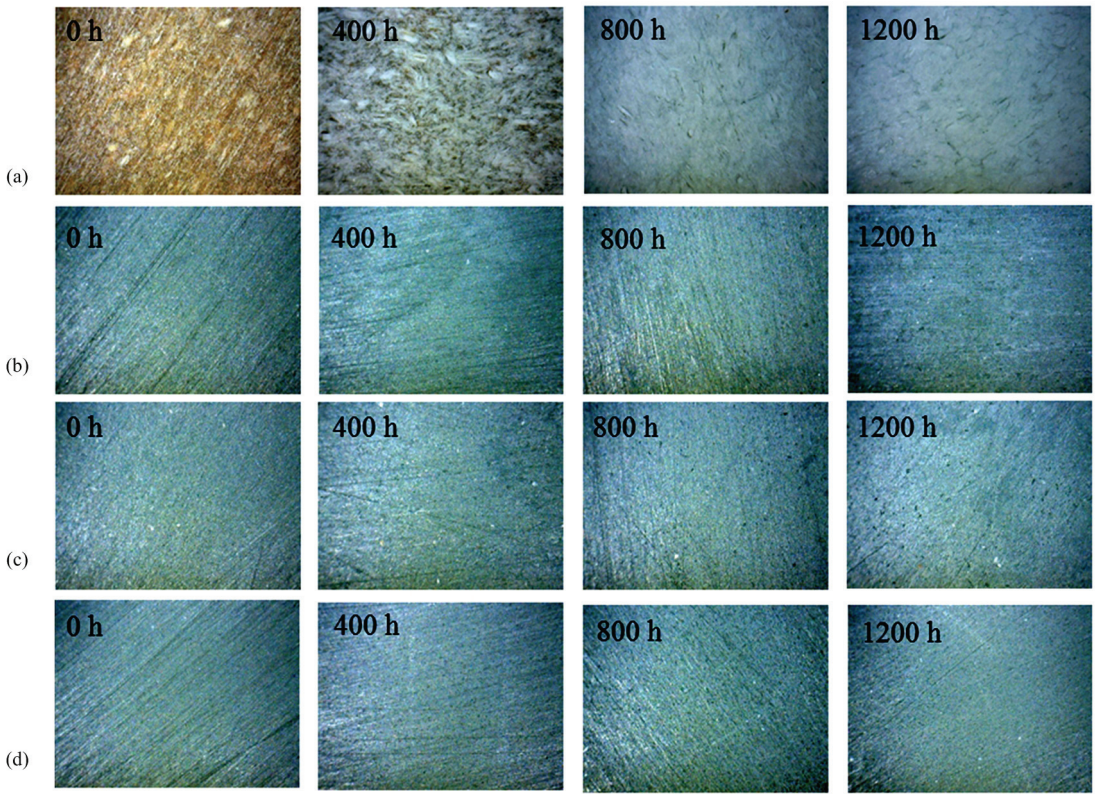

Fig. 8 Light micrographs (20×) of (a) DF composite, (b) WRT composite, (c) AM composite, and (d) NA composite that were xenon-arc-weathered for 0 h, 400 h, 800 h, and 1200 h.

particles could be more effective in improving the UV stability of LLDPE films. These results show that biochar can be used as a light stabilizer in composite materials. The Δa^* (Fig. 9c) and Δb^* (Fig. 9d) of DF composite decreased with the increasing exposure time, showing the greenness and blueness. Noticeably, the Δb^* of pure HDPE slightly increased, which is attributed to the fact that polyolefin degrades under light to show yellowness.

The carbonyl bands, vinyl bands, and hydroxyl groups of weathered DF composite were changed from the FTIR spectra (Fig. 10). The C–O stretching groups of wood cellulose was between 1050 cm^{-1} and 1020 cm^{-1}[68]. The band between 1650 cm^{-1} and 1630 cm^{-1} was attributed to vinyl (C=C) groups[69]. During weathering, the spectra of DF composite showed some bands between 1800 cm^{-1} and 1680 cm^{-1}, which were assigned to the carbonyl functional groups (Fig. 10). The literature shows that the carbonyl groups can be identified into conjugated ketone (1700 cm^{-1} – 1680 cm^{-1}), carboxylic acids (1725 cm^{-1} – 1715 cm^{-1}), ester (1745 – 1730), and γ-lactone (1800 cm^{-1} – 1765 cm^{-1}), which are photolabile[70–73]. The FTIR spectra showed that the carbonyl signals increased, indicating chemical oxidation (Fig. 11). In addition, the carbonyl band was shifted from 1734 cm^{-1} to 1715 cm^{-1} with increasing weathering, indicating that the esters reduced and carbonyl acids formed[74]. The four

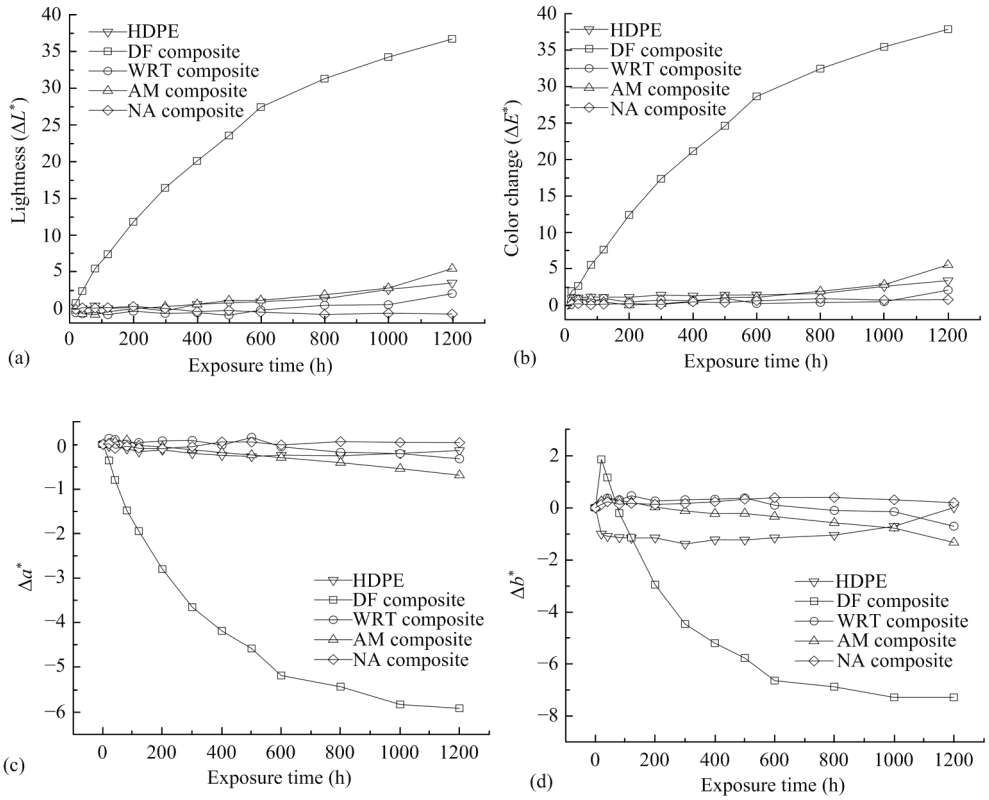

Fig. 9 Effect of xenon-arc accelerated weathering on the (a) lightness (Δ*L*), (b) color change (Δ*E*), (c) redness and greenness (Δ*a**), and (d) yellowness and blueness (Δ*b**) of HDPE and WPC samples.

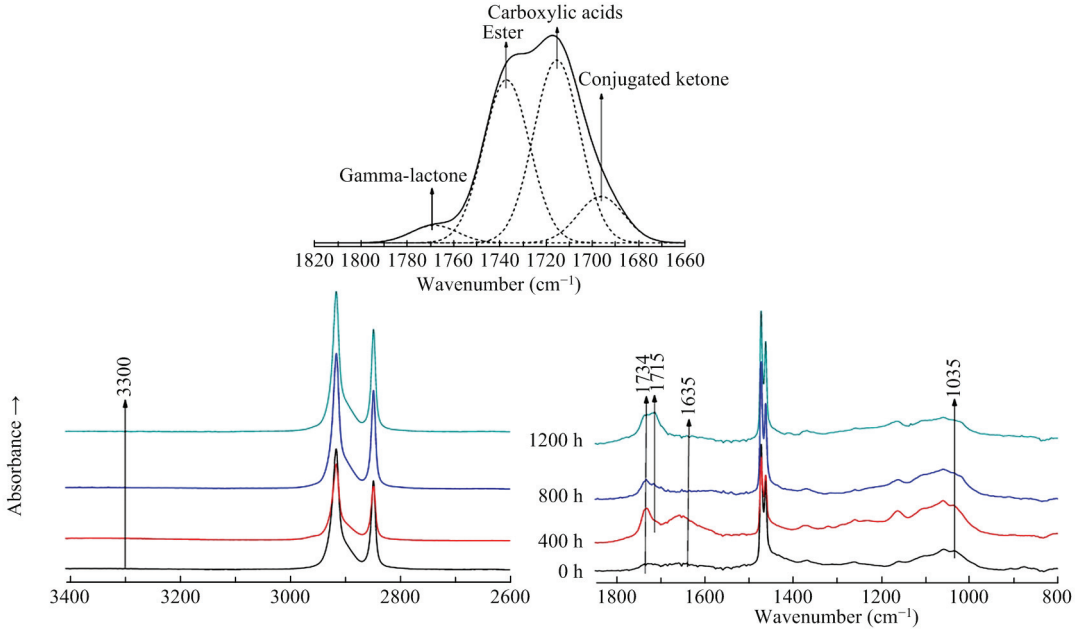

Fig. 10 FTIR spectra of weathered DF composite that were accelerated weathering for 0 h, 400 h, 800 h, and 1200 h.

composites experienced changes in carbonyl content during weathering. DF (Fig. 11a) and WRT (Fig. 11b) composites had similar changes in carbonyl content, so did the AM (Fig. 11c) and NA (Fig. 11d) composites.

In order to determine the extent of the wood composite oxidation, the carbonyl groups (carboxylic acids,

esters and vinyl) were examined based on the Eq. (9). The concentration of carbonyl groups (carboxylic acids and esters) and vinyl groups varied with increasing exposure time (Fig. 12). Both the concentration of carboxyl (carboxylic acid (Fig. 12a) and esters (Fig. 12b)) and vinyl (Fig. 12c) increased with the weathering time firstly, and then decreased. The results were in agreement with concentration reported by Fabiyi *et al*. [70] for the HDPE- and PP-based WPC. Among the composites, the DF composite experienced the most changes of the concentrations, increasing from 0.9 mol·kg^{-1} to 2.3 mol·kg^{-1} for carboxylic acids, 0.6 mol·kg^{-1} to 1.4 mol·kg^{-1} for esters, and 2.4 mol·kg^{-1} to 6.0 mol·kg^{-1} for vinyl groups. The result indicated that HDPE in DF composite experienced more chain cleavage. The changes in carbonyl groups (1800 cm^{-1} – 1680 cm^{-1}) during weathering were measured by calculating *CI* (Fig. 12d). *CI* of all the wood composite increased at the beginning of weathering due to oxidation. However, with the extended exposure time, *CI* reduced probably due to wood loss at the WPC surface. *CI* of DF composite increased from 0.2 to 5.1, which experienced the most changes. While *CI* of NA composite varied from 0.3 to 2.1, indicating more stability. The possible reason is that decreasing the particle size and increasing the specific surface area results in greater stability[75].

4 Conclusion

WPC with four types fibers (DF, WRT biochar, AM biochar and NA carbon) as reinforcing filler were successfully prepared by an extrusion process. The NA composite melts performed higher modulus and viscosity than the other three composites, indicating different melt processability. Tensile properties of NA composite exhibited the best, mainly due to the least extractive content of carbon fiber. The storage modulus of NA composite also displayed the highest values, suggesting the enhanced interfacial interaction as evidenced by adhesion factor. The improved T_s of NA composite further confirmed the stronger interaction between carbon and HDPE matrix. The biochar and carbon composites were more thermally stable than the DF composite. The addition of biochar and carbon also improved the WPC

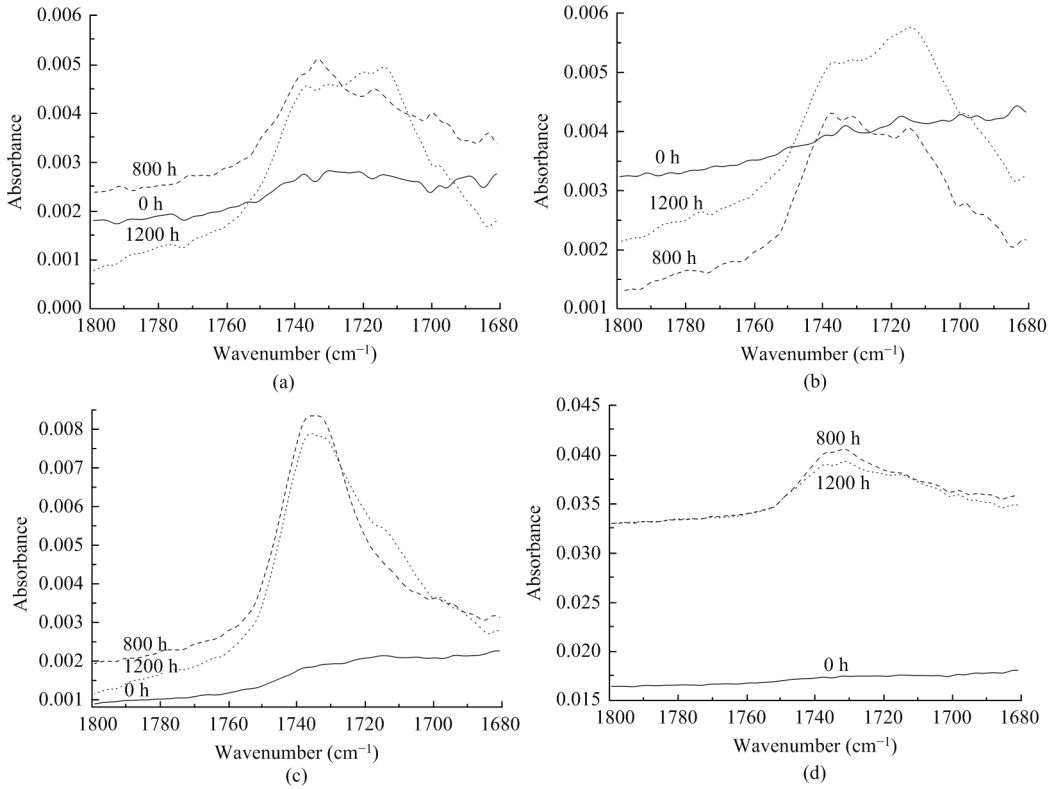

Fig. 11 FTIR spectra of the expanded carbonyl (C=O) region of 0 h, 800 h, and 1200 h of accelerated weathering of (a) DF composite, (b) WRT composite, (c) AM composite, and (d) NA composite.

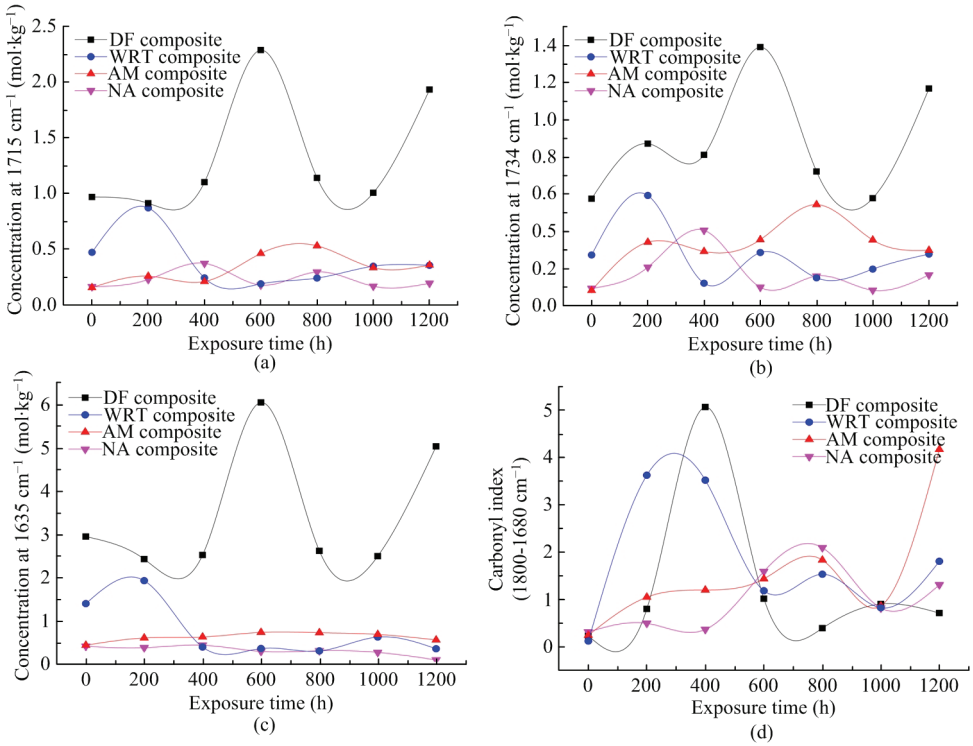

Fig. 12 Effects of accelerated weathering on the concentration of (a) carboxylic acid (1715 cm^{-1}), (b) ester (1734 cm^{-1}), (c) vinyl (1635 cm^{-1}), and (d) carbonyl index in the WPC.

dimensional stability and weathering performance (less lightness and color change). In addition, the NA composite displayed less variable change of carbonyl concentration, indicating improved photostability. Biochar is a suitable substitute for wood fiber in WPC materials with improved performance.

Acknowledgment

This work was supported by China Scholarship Council (No. 201706510025). Additionally, the authors acknowledge (1) Dr. Abdulbaset Alayat for his technical help and surface area measurement, (2) Maged Mohamed for technical help with the accelerated weathering tests, and (3) Farid Sotoudehniakarani for his technical help in the extractions. We also acknowledge the M.J. Murdock Charitable Trust for their support in the purchase of the twin screw extruder and USDA-CSREES grant 2007-34158-17640 for support in the purchase of the DSC and DMA instruments.

References

[1] Li X, Lei B, Lin Z, Huang L, Tan S, Cai X. The utilization of bamboo charcoal enhances wood plastic composites with excellent mechanical and thermal properties. *Materials Design*, 2014, **53**, 419–424.

[2] Peng Y, Wang W, Cao J. Preparation of lignin-clay complexes and its effects on properties and weatherability of wood flour/polypropylene composites. *Industrial & Engineering Chemistry Research*, 2016, **55**, 9657–9666.

[3] Pickering K L, Aruan Efendy M G, Le T M. A review of recent developments in natural fiber composites and their mechanical performance. *Composites Part A*: *Applied Science and Manufacturing*, 2016, **83**, 98–112.

[4] Liu R, Peng Y, Cao J. Thermal stability of organo-montmorillonite-modified wood flour/poly(lactic acid) composites. *Polymer Composites*, 2016, **37**, 1971–1977.

[5] Arao Y, Nakamura S, Tomita Y, Takakuwa K, Umemura T, Tanaka T. Improvement on fire retardancy of wood flour/polypropylene composites using various fire retardants. *Polymer Degradation and Stability*, 2014, **100**, 79–85.

[6] Li X, Lei B, Lin Z, Huang L, Tan S, Cai X. The utilization of organic vermiculite to reinforce wood-plastic composites with higher flexural and tensile properties. *Industrial Crops and Products*, 2013, **51**, 310–316.

[7] Wei L, McDonald A G, Freitag C, Morrell J J. Effects of wood fiber esterification on properties, weatherability and biodurability of wood plastic composites. *Polymer Degradation and Stability*, 2013, **98**, 1348–1361.

[8] Deka B K, Maji T K. Effect of silica nanopowder on the properties of wood flour/polymer composite. *Polymer Engineering and Science*, 2012, **52**, 1516–1523.

[9] Devi R R, Maji T K. Preparation and characterization of wood/styrene-acrylonitrile copolymer/MMT nanocomposite. *Journal of Applied Polymer Science*, 2011, **122**, 2099–2109.

[10] Mwaikambo L Y, Ansell M P. The effect of chemical treatment on the properties of hemp, sisal, jute and kapok for composite reinforcement. *Die Angewandte Makromolekulare Chemie*, 1999, **272**, 108–116.

[11] Lee S H, Wang S. Biodegradable polymers/bamboo fiber biocomposite with bio-based coupling agent. *Composites Part A*: *Applied Science and Manufacturing*, 2006, **37**, 80–91.

[12] Das O, Kim N K, Sarmah A K, Bhattacharyya D. Development of waste based biochar/wool hybrid biocomposites: Flammability characteristics and mechanical properties. *Journal of Cleaner Production*, 2017, **144**, 79–89.

[13] Srinivasan P, Sarmah A K, Smernik R, Das O, Farid M, Gao W. A feasibility study of agricultural and sewage biomass as biochar, bioenergy and biocomposite feedstock: Production, characterization and potential applications. *Science of the Total Environment*, 2015, **512-513**, 495–505.

[14] Kookana R S, Sarmah A K, Van Zwieten L, Krull E, Singh B. Biochar application to soil: Agronomic and environmental benefits and unintended consequences. *Advances in Agronomy*, 2011, **112**, 103–143.

[15] Arni S A. Comparison of slow and fast pyrolysis for converting biomass into fuel. *Renewable Energy*, 2018, **124**, 197–201.

[16] Mohanty P, Nanda S, Pant K K, Naik S, Kozinski J A, Dalai A K. Evaluation of the physiochemical development of biochars obtained from pyrolysis of wheat straw, timothy grass and pinewood: Effects of heating rate. *Journal of Analytical and Applied Pyrolysis*, 2013, **104**, 485–493.

[17] Spiridon I. Natural fiber-polyolefin composites. *Cellulose Chemistry and Technology*, 2014, **48**, 599–612.

[18] Belda R M, Lidón A, Fornes F. Biochars and hydrochars as substrate constituents for soilless growth of myrtle and mastic. *Industrial Crops and Products*, 2016, **94**, 132–142.

[19] Oliveira F R, Patel A K, Jaisi D P, Adhikari S, Lu H, Khanal S K. Environmental application of biochar: Current status and perspectives. *Bioresource Technology*, 2017, **246**, 110–122.

[20] Vaughn S F, Kenar J A, Tisserat B, Jackson M A, Joshee N, Vaidya B N, Peterson S C. Chemical and physical properties of *Paulownia elongata* biochar modified with oxidants for horticultural applications. *Industrial Crops and Products*, 2017, **97**, 260–267.

[21] Margenot A J, Griffin D E, Alves B S Q, Rippner D A, Li C, Parikh S J. Substitution of peat moss with softwood biochar for soil-free marigold growth. *Industrial Crops and Products*, 2018, **112**, 160–169.

[22] Zhang Q, Cai H, Yang K, Yi W. Effect of biochar on mechanical and flame retardant properties of wood – Plastic composites. *Results in Physics*, 2017, **7**, 2391–2395.

[23] Das O, Bhattacharyya D, Hui D, Lau K T. Mechanical and flammability characterisations of biochar/polypropylene biocomposites. *Composites Part B*: *Engineering*, 2016, **106**, 120–128.

[24] DeVallance D B, Oporto G S, Quigley P. Investigation of hardwood biochar as a replacement for wood flour in wood-polypropylene composites. *Journal of Elastomers and Plastics*, 2016, **48**, 510–522.

[25] Ho M, Lau K, Wang H, Hui D. Improvement on the properties of polylactic acid (PLA) using bamboo charcoal particles. *Composites Part B*: *Engineering*, 2015, **81**, 14–25.

[26] Ahmetli G, Kocaman S, Ozaytekin I, Bozkurt P. Epoxy composites based on inexpensive char filler obtained from plastic waste and natural resources. *Polymer Composites*, 2013, **34**, 500–509.

[27] Adefisan O O, McDonald A G. Evaluation of wood plastic composition product from mahogany and teak. *International Journal of Advanced Engineering Research and Science* (*IJAERS*), 2017, **4**, 27–32.

[28] Quirk J T. Cell-wall density of Douglas-fir by two optometric methods. *Wood Fiber Science*, 1984, **16**, 224–236.

[29] Brewer C E, Chuang V J, Masiello C A, Gonnermann H, Gao X, Dugan B, Driver L E, Panzacchi P, Zygourakis K, Davies C A. New approaches to measuring biochar density and porosity. *Biomass & Bioenergy*, 2014, **66**, 176–185.

[30] Fabiyi J S, McDonald A G. Effect of wood species on property and weathering performance of wood plastic composites. *Composites Part A*: *Applied Science and Manufacturing*, 2010, **41**, 1434–1440.

[31] Stark N M, Matuana L M. Surface chemistry changes of weathered HDPE/wood-flour composites studied by XPS and FTIR spectroscopy. *Polymer Degradation and Stability*, 2004, **86**, 1–9.

[32] Nunes C A, Guerreiro M C. Estimation of surface area and pore volume of activated carbons by methylene blue and iodine numbers. *Quimica Nova*, 2011, **34**, 472–476.

[33] Clemons C M, Stark N M. Feasibility of using saltcedar as a filler in injection-molded polyethylene composites. *Wood*

Fiber Science, 2009, **41**, 2–12.

[34] Gallagher L W, McDonald A G. The effect of micro sized wood fibers in wood plastic composites. *Maderas-Ciencia Y Tecnologia*, 2013, **15**, 357–374.

[35] Hristov V, Takács E, Vlachopoulos J. Viscoelastic behavior of highly filled HDPE/wood flour composites. *ANTEC*, 2005, 1331–1335.

[36] Luo S, Cao J, McDonald A G. Interfacial improvements in a green biopolymer alloy of poly(3-hydroxybutyrate-co-3-hydroxyvalerate) and lignin *via in situ* reactive extrusion. *ACS Sustainable Chemistry & Engineering*, 2016, **4**, 3465–3476.

[37] Marcovich N E, Reboredo M M, Kenny J M, Aranguren M. Rheology of particle suspensions in viscoelastic media. Wood flour-polypropylene melt. *Rheologica Acta*, 2004, **43**, 293–303.

[38] Hristov V, Takács E, Vlachopoulos J. Surface tearing and wall slip phenomena in extrusion of highly filled HDPE/wood flour composites. *Polymer Engineering and Science*, 2006, **46**, 1204–1214.

[39] Ou R, Xie Y, Wolcott M P, Yuan F, Wang Q. Effect of wood cell wall composition on the rheological properties of wood particle/high density polyethylene composites. *Composites Science and Technology*, 2014, **93**, 68–75.

[40] Belaïd S, Boiteux G, Cassagnau P. Rheological and electrical properties of EVA copolymer filled with bamboo charcoal. *Rheologica Acta*, 2013, **52**, 75–84.

[41] Stark N M, Rowlands R E. Effects of wood fiber characteristics on mechanical properties of wood/polypropylene composites. *Wood and Fiber Science*, 2003, **35**, 167–174.

[42] Ikram S, Das O, Bhattacharyya D. A parametric study of mechanical and flammability properties of biochar reinforced polypropylene composites. *Composites Part A*: *Applied Science and Manufacturing*, 2016, **91**, 177–188.

[43] Das O, Sarmah A K, Bhattacharyya D. A novel approach in organic waste utilization through biochar addition in wood/polypropylene composites. *Waste Management*, 2015, **38**, 132–140.

[44] Zhang Q, Yi W, Li Z, Wang L, Cai H. Mechanical properties of rice husk biochar reinforced high density polyethylene composite. *Polymers*, 2018, **10**, 286–295.

[45] Ren W, Zhang D, Wang G, Cheng H. Mechanical and thermal properties of bamboo pulp fiber reinforced polyethylene composites. *Bioresources*, 2014, **9**, 4117–4127.

[46] Wang C, Yu X, Smith L M, Wang G, Cheng H, Zhang S. Interfacial properties of bamboo fiber-reinforced high-density polyethylene composites by different methods for adding nano calcium carbonate. *Polymers*, 2017, **9**, 587–600.

[47] Tian S, He H, Yu P, Zhou L, Luo Y, Jia D. Sustainable utilization of waste printed circuit boards powders in HDPE-wood composites: Synergistic effects of multicomponents on structure and properties. *Journal of Cleaner Production*, 2017, **164**, 840–847.

[48] Kubát J, Rigdahl M, Welander M. Characterization of interfacial interactions in high density polyethylene filled with glass spheres using dynamic-mechanical analysis. *Journal of Applied Polymer Science*, 1990, **39**, 1527–1539.

[49] Luo S, Cao J, McDonald A G. Esterfication of industrial lignin and its effect on the resulting poly(3-hydroxybutyrate-co-3-hrdroxyvalerate) or polypropylene blends. *Industrial Crops and Products*, 2017, **97**, 281–291.

[50] Debenedetti P G, Stillinger F H. Supercooled liquids and the glass transition. *Nature*, 2001, **410**, 259–267.

[51] Xu X, Liu F, Jiang L, Zhu J Y, Haagenson D, Wiesenborn D P. Cellulose nanocrystals vs. cellulose nanofibrils: A comparative study on their microstructures and effects as polymer reinforcing agents. *ACS Applied Materials & Interfaces*, 2013, **5**, 2999–3009.

[52] Yu H Y, Qin Z Y, Yan C F, Yao J M. Green nanocomposites based on functionalized cellulose nanocrystals: A study on the relationship between interfacial interaction and property enhancement. *ACS Sustainable Chemistry & Engineering*, 2014, **2**, 875–886.

[53] Lu H, Nutt S. Restricted relaxation in polymer nanocomposites near the glass transition. *Macromolecules*, 2003, **36**, 4010–4016.

[54] Sun F, Huang H. Rheology and thermal properties of polypropylene modified by reactive extrusion with dicumyl peroxide and trimethylol propane triacrylate. *Advances in Polymer Technology*, 2009, **28**, 16–25.

[55] Cui Y H, Tao J, Noruziaan B, Cheung M, Lee S. DSC analysis and mechanical properties of wood-plastic composites. *Journal of Reinforced Plastics and Composites*, 2010, **29**, 278–289.

[56] Das O, Sarmah A K, Zujovic Z, Bhattacharyya D. Characterisation of waste derived biochar added biocomposites: Chemical and thermal modifications. *Science of The Total Environment*, 2016, **550**, 133–142.

[57] Ndiaye D, Dipo B, Thiandoume C, Fall P A, Farota A K, Tidjani A. Morphology and thermo mechanical properties of wood/polypropylene composites. In: Dogan F (ed.), *Polypropylene*, InTech Open Access, London, UK, 2012, 415–428. DOI: 10.5772/36148

[58] Ouajai S, Shanks R A. Composition, structure and thermal degradation of hemp cellulose after chemical treatments. *Polymer Degradation and Stability*, 2005, **89**, 327–335.

[59] Essabir H, Hilali E, Elgharad A, Minor H E, Imad A, Elamraoui A, Gaoudi O Al. Mechanical and thermal properties of bio-composites based on polypropylene reinforced with nut-shells of argan particles. *Materials & Design*, 2013, **49**, 442–448.

[60] Ahmad E E M, Luyt A S. Effects of organic peroxide and polymer chain structure on morphology and thermal properties of sisal fiber reinforced polyethylene composites. *Composites Part A*: *Applied Science and Manufacturing*, 2012, **43**, 703–710.

[61] Zhang Y, Ma Z, Zhang Q, Wang J, Ma Q, Yang Y, Luo X, Zhang W. Comparison of the physicochemical characteristics of bio-char pyrolyzed from Moso bamboo and rice husk with different temperatures. *Bioresources*, 2017, **12**, 4652–4669.

[62] Meng X, Zhang Y, Lu J, Zhang Z, Liu L, Chu P K. Effects of bamboo charcoal power on the curing characteristics, mechanical properties, and thermal properties of styrene-butadiene rubber with bamboo charcoal power. *Journal of Applied Polymer Science*, 2013, **130**, 4534–4541.

[63] Abdul Khalil H P S, Firoozian P, Bakare I O, Akil H M, Noor A M. Exploring biomass based carbon black as filler in epoxy composites: Flexural and thermal properties. *Materials & Design*, 2010, **31**, 3419–3425.

[64] Li S, Li X, Chen C, Wang H, Deng Q, Gong M, Li D. Development of electrically conductive nano bamboo charcoal/ultra-high molecular weight polyethylene composites with a segregated network. *Composites Science and Technology*, 2016, **132**, 31–37.

[65] Fabiyi J S, McDonld A G, Morrell J J, Freitag C. Effects of wood species on durability and chemical changes of fungal decayed wood plastic composites. *Composites Part A*: *Applied Science and Manufacturing*, 2011, **42**, 501–510.

[66] Javadi Y, Hosseini M S, Aghjeh M K R. The effect of carbon black and HALS hybrid systems on the UV stability of high-density polyethylene (HDPE). *Iranian Polymer Journal*, 2014, **23**, 793–799.

[67] Liu M, Horrocks A R. Effect of carbon black on UV stability of LLDPE films under artificial weathering conditions. *Polymer Degradation and Stability*, 2002, **75**, 485–499.

[68] Faix O. Fourier transform infrared spectroscopy. in: Lin S Y, Dence C W, eds. *Methods in Lignin Chemistry*. Springer, Berlin, Germany, 1992, 83–109.

[69] Miller F A. Characteristic frequencies of alkenes (olefins). In: Mayo D W, Miller F A, Hannah R W, eds. *Course Notes on the Interpretation of Infrared and Raman Spectra*. John Wiley & Sons, New York, USA, 2003, 73–84.

[70] Fabiyi J S, McDonald A G, Wolcott M P, Griffiths P R. Wood plastic composites weathering visual appearance and chemical changes. *Polymer Degradation and Stability*, 2008, **93**, 1405–1414.

[71] Lacoste J, Carlsson D J, Falicki S, Wiles D M. Polyethylene hydroperoxide decomposition products. *Polymer Degradation and Stability*, 1991, **34**, 309–323.

[72] Mayo D W. Spectra of carbonyl compounds of all kinds (factors affecting carbonyl group frequencies). In: Mayo D W, Miller F A, Hannah R W, eds. *Course Notes on the Interpretation of Infrared and Raman Spectra*, John Wiley & Sons, New York, USA, 2003, 179–204.

[73] Stark N M, Matuana L M, Clemons C M. Effect of processing method on surface and weathering characteristics of wood-flour/HDPE composites. *Journal of Applied Polymer Science*, 2004, **93**, 1021–1030.

[74] Evans P D, Owen N L, Schmid S, Webster R D. Weathering and photostability of benzoylated wood. *Polymer Degradation and Stability*, 2002, **76**, 291–303.

[75] Peña J M, Allen N S, Edge M, Liauw C M, Valange B. Studies of synergism between carbon black and stabilisers in LDPE photodegradation. *Polymer Degradation and Stability*, 2001, **72**, 259–270.